Magnetic order effects on the electronic structure of KMMnS_{2}(M=Cu,Li) with the ThCr_{2}Si_{2}-type structure

Austin Virtue, Xiuquan Zhou, Brandon Wilfong, Jeffrey W. Lynn, Keith Taddei, Peter Zavalij, Limin Wang, and Efrain E. Rodriguez

Phys. Rev. Materials **3**, 044411 — Published 30 April 2019

DOI: 10.1103/PhysRevMaterials.3.044411

Magnetic order effects on the electronic structure of KMMnS$_2$ (M = Cu, Li) with the ThCr$_2$Si$_2$-type structure

Austin Virtue,[1] Xiuquan Zhou,[1] Brandon Wilfong,[1,2] Jeffrey W. Lynn,[3]
Keith Taddei,[4] Peter Zavalij,[1] Limin Wang,[2] and Efrain E. Rodriguez[1,2,*]

[1] *Department of Chemistry and Biochemistry, University of Maryland, College Park, Maryland 20742, United States*
[2] *Center for Nanophysics and Advanced Materials, University of Maryland, College Park, Maryland 20742, United States*
[3] *NIST Center for Neutron Research, National Institute of Standards and Technology, Gaithersburg, MD 20899-6102, USA*
[4] *Neutron Scattering Division, Oak Ridge National Laboratory, Oak Ridge, Tennessee 37831, USA*

We study the relationship between antiferromagnetic order and the electronic properties of KCuMnS$_2$ with the ThCr$_2$Si$_2$-type structure. We propose two magnetic structures for KCuMnS$_2$ with the ThCr$_2$Si$_2$-type structure. Powder samples of KCuMnS$_2$ and KLiMnS$_2$ were prepared for structural studies and magnetization measurements. In both compounds, the Mn^{2+} site is alloyed by either Cu$^+$ or Li$^+$. We also prepared single crystals of KCuMnS$_2$ for x-ray and neutron diffraction studies and resistivity measurements. We relate these properties to the electronic structure calculated with density functional theory. Neutron diffraction studies reveal that KCuMnS$_2$ exhibits long-range magnetic ordering with a Néel temperature near 160 K and a moment of 0.92(2) μ_B/ Mn^{2+} at 6 K. In contrast, KLiMnS$_2$ never exhibits long-range magnetic ordering down to 3.5 K. Both sulfides never display a crystallographic phase transition from our temperature-dependent x-ray and neutron diffraction studies. We discuss the magnetic phases in detail and how they relate to isostructural phases such as iron-based superconductors and related chalcogenides. Electrical resistance measurements indicate that while KCuMnS$_2$ is semiconducting, there is an anomaly around the Néel temperature, which indicates that long range magnetism influences its electronic structure.

I. INTRODUCTION

The ThCr$_2$Si$_2$-structure type (Figure 1), also known as the 122-type in the condensed matter physics literature, represents a large collection of layered compounds that can incorporate much of the periodic table and therefore exhibit a variety of physical phenomena.[1,2] For example, the 122-type pnictides (Pn) and chalcogenides (Ch) with iron have attracted significant amount of attention because of their superconducting properties. The BaFe$_2$As$_2$ parent compound can be either aliovalently or isovalently doped to a superconductor from an antiferromagnetic semimetal.[3–6] The structurally related K$_x$Fe$_{2-y}$Se$_2$ can also express superconductivity, although it is always mixed with an antiferromagnetic, insulating phase due to the distribution of iron vacancies.[7–9]. The origin of superconductivity in both pnictides and chalcogenides is still on-going research, and several implied mechanisms including spin fluctuations and nematic electronic states have been proposed.[10–14]

Due to the proximity to Fe, we first explore Mn chalcogenides in the 122-type structure to find similar ground states. The ACo_2X_2 series (where X = Pn or Ch and A is an alkali or alkaline earth metal) tend to express long-range ferromagnetic order.[15–19] For Mn, the magnetism of its 122-type pnictides, such as BaMn$_2$As$_2$, has been well studied, included by neutron diffraction.[20–22] However, the ternary 122-type Mn chalcogenides are unknown. Likely, this arises from charge balance arguments. By replacing As^{3-} with Se^{2-}, one must reduce Mn below the +2 oxidation state, which is difficult to do for the stable d^5 transition metal. However, Mn^{2+} can be incorporated into quaternary 122-type chalcogenides by alloying it with a monovalent cation such as

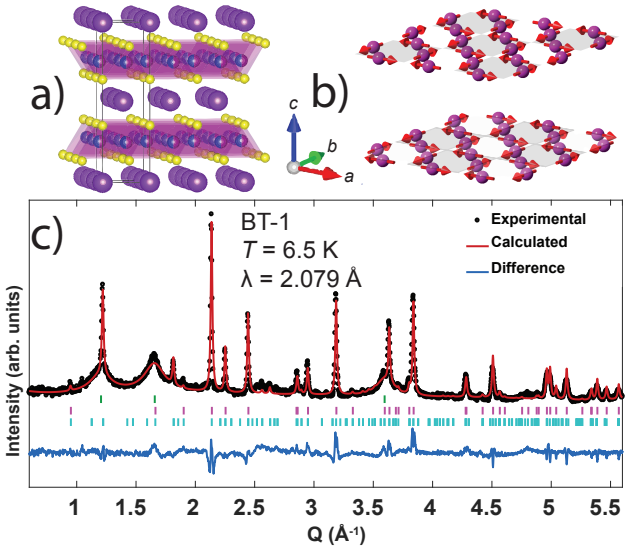

FIG. 1. Chemical and plausible magnetic structure of KCuMnS$_2$ from neutron powder diffraction. (a) Atomic structure with equal occupancy of Cu/Mn sites (blue and magenta) forming two-dimensional sulfide (yellow) tetrahedral layers separated by potassium (purple) cations. b) A proposed antiferromagnetic pinwheel magnetic structure of KCuMnS$_2$, showing only the magnetic Cu/Mn site, with the moment in the ab-plane. This is one of two magnetic structure that fit equally as well to NPD data. (c) Rietveld refinement fit to neutron powder diffraction data (R_{wp} = 7.211 %) with magnetic phase (bottom ticks), structural phase (middle ticks), and impurity peaks (top ticks) indicated.

Cu^+ or Li^+.[23] Indeed, ACuMnCh_2 and ALiMnCh_2 have been reported in the pioneering work of Greenblatt[24–28] and Bronger,[29,30] respectively. Unlike the ternary 122-type pnictides, no long-range magnetic ordering was found for ACuMnCh_2 compounds in earlier studies,[24,25] and no physical property measurements carried out for ALiMnCh_2.[29]

Due to the lack of neutron diffraction data for these quaternary Mn chalcogenides in previous studies, their underlying magnetic order remains unknown. Hence, more comprehensive studies are needed to elucidate their relationship to structurally related Fe-based superconductors. This is crucial for any attempt to find a new non-Fe based system that can exhibit superconductivity. We focus here on the sulfides of Mn with the A cation being K^+. Any future studies on tuning the properties of quaternary Mn sulfides through doping would require an understanding of 1) the underlying magnetic order, 2) the ideal synthetic and crystal growth conditions, and 3) the electronic and transport properties. We therefore reinvestigate and present the preparation, single crystal growth, chemical and magnetic structures, and ground state properties of these 122-type quaternary phases.

II. EXPERIMENTAL AND COMPUTATIONAL METHODS

The quaternary sulfides were prepared by heating a mixture of pure metals with alkali metal carbonates under a flow of argon charged with carbon disulfide (99.9% ACS reagent grade, Aldrich). Depending on the desired product, stoichiometric amounts of Mn metal (99.95% -325 mesh, Alfa Aesar) were mixed with either Cu metal (99.5% -200 +325 mesh, CERAC inc.) or a 5% excess of lithium carbonate (98%, Honeywell) to account for some Li evaporation, along with a 10% excess of potassium carbonate (99% anhydrous, Alfa Aesar). Powders were ground together in an agate mortar and pestle as an acetone slurry to a homogeneous mixture and allowed to dry. A typical synthesis of 12.5 mmol would consist of 0.9502 g K_2CO_3, 0.4849 g Li_2CO_3, 0.7943 g Cu, 0.6867 g Mn, and approximately 15 mL of CS_2.

The mixture was loaded as a powder into an alumina crucible which was then placed into a tube furnace under a flow of argon. The mixed gas flow pathway was set up to flow into and out of a three neck flask before entering the furnace, exiting the tube furnace through a bleach solution. The furnace was then heated at a rate of 180 °C per hour up to 800 °C. Once the temperature was reached, a fifteen fold excess of carbon disulfide was added via syringe to the three neck flask as a liquid and allowed to evaporate into the argon flow. Following complete evaporation of the carbon disulfide, the sample was cooled to room temperature at 180 °C per hour.

CAUTION: to impede the evolution of toxic H_2S, the end of the CS_2 stream was bubbled through a bleach solution (concentrated Clorox germicidal bleach, active ingredient: 8.25% sodium hypochlorite). The entire apparatus was contained in a fume hood.

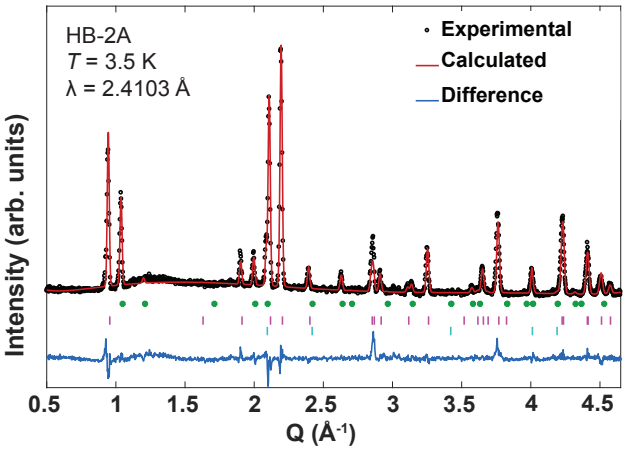

FIG. 2. Rietveld refinement of the structure of $KLiMnS_2$ with neutron diffraction powder diffraction data at 3.5 K, $R_{wp} = 7.019$ %. Top tick marks are for $KLiMnS_2$ and bottom tick marks for the MnS alabandite impurity with its magnetic peaks indicated by circles.

The powders recovered contained impurities of potassium polysulfide as well as an additional impurity of alabandite for the Li sample. This polysulfide impurity could either be washed away with small amounts of water followed by methanol, or used as the flux for single crystal growth of the Cu compound, described below.

Single crystal growth was achieved by placing roughly 0.25 g of the unwashed powder into an evacuated quartz ampule, which was then placed in a second evacuated quartz ampule, heated at a rate of 50 °C per hour to 1000 °C. This temperature was held for 10 hours before cooling at a rate of 6 °C per hour to 500 °C. The ampule was then cooled at a rate of 30 °C per hour to room temperature. Single crystals were then recovered manually.

Neutron powder measurements for $KCuMnS_2$ were performed on the BT-1 diffractometer at the NIST Cen-

TABLE I. Single-crystal X-ray diffraction data for KCuMnS_2.

Space Group	$I4/mmm$ (no.139)
a (Å)	3.9442(8)
c (Å)	13.239(3)
Crystal system	Tetragonal
Volume (Å^3)	205.96(9)
Z	2
Calculated density (g cm^{-3})	3.575
λ, Mo Kα Å	0.71073
No. of reflections collected	1080
No. of independent reflections	133
$F(000)$	210.0
R_1, wR_2 (%)	2.01, 4.31
Temperature	110 K

TABLE II. Structural, lattice, and anisotropic displacement parameters for $I4/mmm$ $KCuMnS_2$ from single crystal data at 110 K. All off-diagonal terms are equal to zero.

Atom	Wyckoff Site	x	y	z	$U_{11}(Å^2) = U_{22}(Å^2)$	$U_{33}(Å^2)$
K	2a	0	0	0.5	0.0118(4)	0.0158(7)
Cu/Mn	4d	0.5	0	0.75	0.0071(2)	0.0153(3)
S	4e	0.5	0.5	0.35607(9)	0.0071(3)	0.0121(5)

ter for Neutron Research (NCNR) with wavelength $\lambda = 2.079$ Å (Ge 311 monochromator) at a base temperature of 6 K. Temperature dependence of the magnetic peak centered at approximately 1.24 $Å^{-1}$ was carried out on a single crystal with the position sensitive detector on the BT-7 triple-axis spectrometer (NCNR)[31] with a wavelength $\lambda = 2.359$ Å from 10 to 220 K. Neutron powder measurements for $KLiMnS_2$ were performed on the HB-2A diffractometer at the Oak Ridge National Laboratory, High Flux Isotope Reactor (HFIR), with wavelength $\lambda = 2.4103$ Å (Ge 113 monochromator). Temperature dependent powder diffraction patterns were take starting from a base temperature of 3.5 K. Symmetry analysis was perfomred using ISODISTORT from the ISOTROPY web-based software suite.[32] Rietveld refinements of the neutron diffraction data was carried out using the TOPAS 5.0 software.[33]

X-ray data was collected on a $KCuMnS_2$ single crystal of approximate dimensions 0.29 mm × 0.13 mm × 0.04 mm in size with Mo Kα radiation of $\lambda = 0.71073$ Å. The crystal was measured every 20 degrees from 110 K to 250 K using the Bruker Smart Apex-II CCD system to uncover any possible crystallographic phase transitions coinciding with the onset of long-range magnetic order. The structure was solved and refined with the SHELX Software Package.[34]

Electrical transport measurements were preformed using a 9 T Quantum Design Physical Property Measurement System (PPMS-9) with polycrystalline and single crystal samples of $KCuMnS_2$. Polycrystalline samples were ground into a powder and pressed into pellets utilizing < 2 ton uniaxial load without sintering. Electrical resistivity was measured using the four-probe method with gold wire and contacts made with silver paste. The temperature and field dependence of longitudinal electrical resistivity was measured in a range from 300 K to 1.8 K with applied current of 0.1 mA and frequencies near 17 Hz.

Temperature dependent DC (direct current) magnetic susceptibility measurements were carried out using a Quantum Design Magnetic Property Measurement System (MPMS) on powder samples of $KCuMnS_2$ and $KLiMnS_2$. Field-cooled (FC) and zero field-cooled (ZFC) measurements were taken from 1.8 K to 300 K with an applied magnetic field of 500 Oe. Magnetization versus field loops were carried out using the MPMS from -7 T to 7 T on the powder samples at 2 K and 50 K.

Initial density functional theory (DFT)[35,36] calcula-

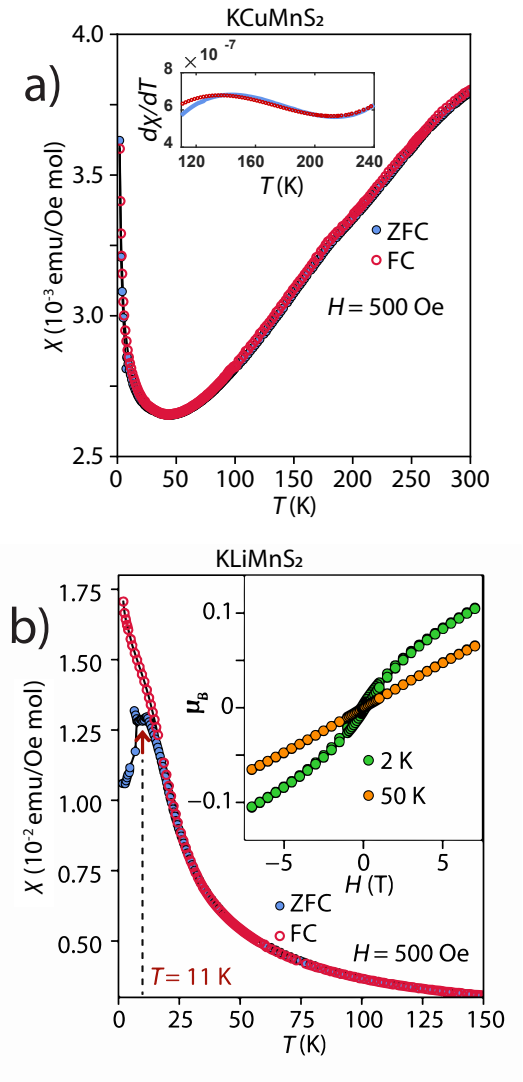

FIG. 3. Temperature dependent magnetic susceptibility of a) $KCuMnS_2$ and b) $KLiMnS_2$. Inset of (a) is the derivative of the susceptibility and shows a subtle feature around the Néel temperature of 160 K. (Conversion to SI units: 1 Oe = $(1000/4\pi)$ A/m, 1 emu/(mol Oe) = $4\pi\ 10^{-6}$ m^3/mol)

tions for a simple layered Néel type magnetic structure were performed by using the Vienna Abinitio Simulation Package (VASP)[37–40] software package with potentials using the projector augmented wave (PAW)[41] method. The exchange and correlation functional were treated by

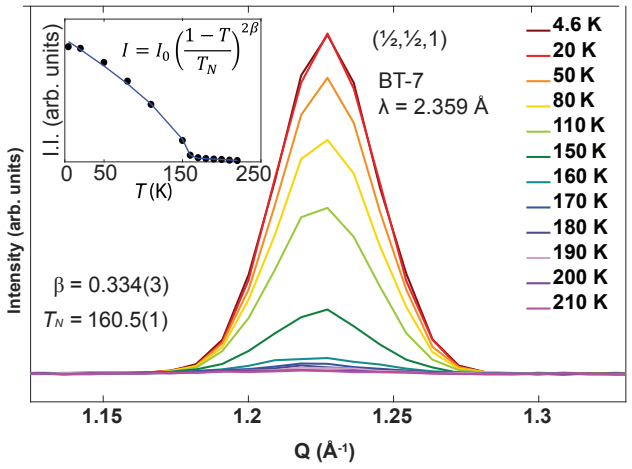

FIG. 4. Temperature dependence of a magnetic Bragg peak in a single crystal sample of KCuMnS2 from neutron diffraction. (inset) The integrated intensity of the peak is plotted versus temperature in order to fit the magnetic order parameter. From the least-squares fit we extract a Néel temperature close to 160.5(1) K and a critical exponent β of 0.334(3).

the generalized gradient approximation (PBE-GGA).[42] The cutoff energy, 450 eV, was applied to the valence electronic wave functions expanded in a plane-wave basis set for all chalcogenides. A MonkhorstPack[43] generated 21 × 21 × 7 k-point grid was used for the Brillouin-zone integration to obtain accurate electronic structures.

In order to demonstrate the effects of the AFM order on the electronic structure for $KCuMnS_2$, the nonmagnetic and magnetic DFT calculations are conducted using VASP with the projector-augmented wave basis in the generalized gradient approximation. The enlarged 2 × 2 magnetic unit cells are shown in Figure S2, which correspond to the stripe-like and non-collinear AFM order suggested by our neutron experiment. The cut-off energy, 450eV, was applied and the gamma-centered k mesh was taken to be 9 × 9 × 7 and 21 × 21 × 7 for the magnetic and nonmagnetic cases, respectively.

III. RESULTS

A. Crystal structure

Details of the X-ray measurement results on the $KCuMnS_2$ single crystal are gathered in Table I, which shows that the sample crystallizes in a body-centered tetragonal crystal system. The lattice constants are a = 3.9442(8) Å and c = 13.239(3) Å at 110 K in space group $I4/mmm$ (No. 139). Structural parameters are presented in Table II. All occupancies refined to unity. The Cu and Mn atoms share half of the 4d Wyckoff position, which has a site symmetry of $-4m2$. No superlattice reflections that would imply any ordering of the Mn and Cu atoms on the 4d site were observed. The crystal was found to retain tetragonal symmetry at all temperatures measured. Temperature dependence of the lattice parameters from single crystal data did not reveal any structural anomaly from 110 K to 250 K (See Figure S1 in Supplementary Information).

The structure obtained from the single crystal X-ray results (Tables I and II) was used to model and fit the neutron powder diffraction (NPD) data. The NPD pattern revealed extra reflections at base temperature, which we attribute to antiferromagnetic ordering. These satellite reflections were indexed with a propagation vector of $\mathbf{k} = (\frac{1}{2}, \frac{1}{2}, 1)$, and are discussed in the next section.

The $KCuMnS_2$ neutron powder sample contained an unknown impurity causing three broad background peaks in the BT-1 data. Likely, the impurity in the powder sample is a either a poorly crystalline sulfide or elemental sulfur that could not be washed away. These broad, and likely amorphous, peaks were fit with three Gaussian peak profiles that may be attributed to the same impurity as they all possessed the same peak profile parameters. Refinement of the structural model shown in Figure 1c with an R_{wp} = 7.211 % indicates full occupancy of all sites in the structure. From NPD, the lattice constants were refined to a = 3.9405(2) Å, c = 13.215(1) Å at 6 K. From temperature dependent NPD measurements, we did not detect any break of the tetragonal symmetry.

Changing the monovalent cation from Cu to Li subtly effects the crystal structure as obtained from Rietveld refinement with the NPD data at 3.5 K (Figure 2) . The compound retains the tetragonal structure but the a parameter lengthens to 4.0312(2) Å (from 3.9405(2) Å in Cu) while the c parameter contracts to 13.1453(8) Å. Using isotopically pure ^{7}Li the NPD is fit nicely with the 122-structure along with a less than 5 wt. % MnS alabandite impurity. At 200 K, without the additional magnetic peaks to index, the occupancy of the 4d site refines to 0.489(6) with Mn and 0.48(1) with Li, leading to a site roughly 97 % occupied. Likely, the loss of Li from evaporation leads to the alabandite impurity. Nevertheless, increasing the initial amounts of Li carbonate did not diminish the amount of alabandite impurity.

B. Magnetism and magnetic structure

First, we report the results from the magnetization measurements. For both powder and single crystal samples of $KCuMnS_2$, the magnetic susceptibilities display similar features. The susceptibility in Figure 3a decreases as the temperature is lowered and no clear cusp in the curve is observed down to 2 K. At 40 K, a Curie tail appears. However, the derivative of the fits to both the zero-field cooled (ZFC) and field cooled (FC) curves, reveals a subtle feature near 160 K. When fit to a polynomial between 100 and 250 K, the first-derivate (Figure 3a inset) of temperature-dependent magnetic susceptibility remained fairly constant (above 40 K). Therefore, it is likely that the system displays some low dimensional

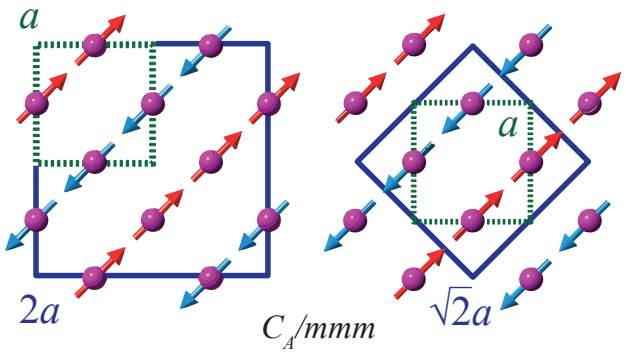

FIG. 5. Proposed striped phase, C_A/mmm magnetic structure of $KCuMnS_2$ with Mn atoms. Structural lattice is shown with green short dashed line, magnetic cell is shown as both the $2a\times2a$ (left) and the $\sqrt{2}a\times\sqrt{2}a$ (right) of the structural cell with blue solid line.

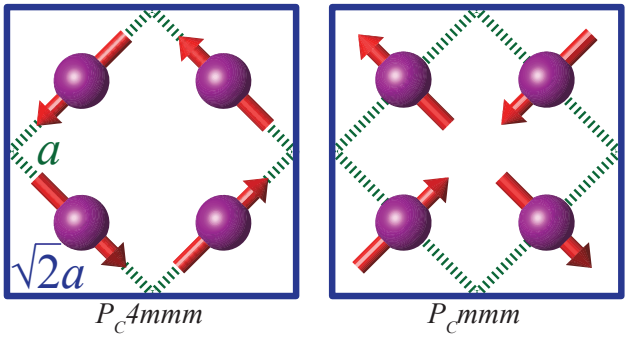

FIG. 6. Alternate non-collinear magnetic phases for $KCuMnS_2$. The P_C4mmm (left) phase, and the P_Cmmm (right) magnetic structure of $KCuMnS_2$ with Mn atoms. Structural lattice is shown with green dashed line, magnetic cell is shown with blue solid line (rotated 45° from Figure 5).

magnetic coupling or competition between multiple magnetic structures that almost completely flatten the cusp-type feature typical of 3D antiferromagnets.[45–48]

In order to elucidate any possible magnetic ordering in $KCuMnS_2$, we performed temperature dependent NPD and single crystal neutron diffraction (BT-7). As shown in Figure 4, the onset of long-range order occurs around 160 K from the magnetic peak centered around 1.24 $Å^{-1}$. The peak was fit to a Gaussian, and the parameters of the profile shape were analyzed as a function of temperature. The integrated intensity (II) *vs.* T is shown in the inset of Figure 4. Fitting the order parameter of magnetization M, which scales with $\sqrt{II}$, yielded a Néel temperature $T_N = 160.5(1)$ K and a critical exponent of $\beta = 0.334(3)$, which is close to the β of a 3D Ising system (0.3264).

From the propagation vector of $\mathbf{k} = (\frac{1}{2}, \frac{1}{2}, 1)$, three plausible space groups for the antiferromagnetic order were proposed. First, the so-called striped phase is presented in Figure 5. Here, the moments on the Mn^{+2} ions align in a stripe pattern with alternating layers oriented antiferromagnetically. This magnetic structure can be fit with magnetic space group C_A/mmm (65.489). A view of the magnetic moments and Mn sites from the c axis (Figure 5) shows that the magnetic unit cell (large, blue dashes) can be thought of as a $2a\times2a$ cell of the chemical unit cell (small green dashes). A further simplified magnetic cell can be adjusted to a $\sqrt{2}a\times\sqrt{2}a$ cell, which then has the symmetry of magnetic space group C_A/mmm.

The other two possible magnetic symmetries are non-collinear ones and are presented in Figure 6. Interestingly, these two models give an identical fit to the NPD data to that of the striped phase. Magnetic space groups P_C4mmm (123.349) and P_Cmmm (47.255) retain the same unit cell ($\sqrt{2}a\times\sqrt{2}a$) as the proposed C_A/mmm structure detailed above but lead to a non-collinear arrangement of the moments. The structures for P_C4mmm and P_Cmmm provide identically good fits to the NPD data, which is to be expected as they are ultimately the same magnetic structure displaced by $\frac{a}{2}+\frac{a}{2}$. However, P_C4mmm does preserve 4-fold symmetry within the unit cell whereas the other does not. As with the striped structure, the magnetic moments of the Mn cations lie only in the ab-plane and are antiferromagnetically coupled between the alternating layers (*i.e.* along the c-axis) as shown in Figure 1b. When comparing the two possible magnetic structures to one another, it is important to recall that the occupancy of the magnetic site is only half Mn with no evidence of long-range ordering of Mn and Cu cations.

Since the system remains tetragonal below the magnetic transition temperature, we can only measure the directional cosine angle of the magnetic moment with respect to the ab-plane. For all three models, however, the moment is only along the ab-plane. At 3.5 K, the moment size refined to 0.462(9) μ_B for the Cu/Mn site. Given that Cu^+ is a d^{10} cation, we can infer that the moment is solely from the Mn cation. Attributing for the occupancy of the site, the moment therefore refines to 0.92(2) μ_B/ Mn^{2+}. This moment size is still approximately 20 % of that anticipated for a d^5 cation.

Upon changing the monovalent cation, the magnetic properties are dramatically altered. At low temperature patterns of the NPD data in Figure 2, strong magnetic peaks were observed, however, none of these actually belonged to $KLiMnS_2$. All could be successfully attributed to the magnetic peaks from the alabandite rock-salt cubic structure which is well known for both MnS and MnO.[49–53]. A broad hump that appears centered around 1.25 $Å^{-1}$ could indicate some short-range ordering with a lack of long-range ordering of the magnetic moments. However, this extra scattering could also arise from inelastic scattering and we cannot therefore definitively assign it to a spin glassy state in $KLiMnS_2$. Although powder samples of $KLiMnS_2$ (Figure 3b) show a cusp in the magnetic susceptibility below 11 K, this may not lead to long-range order as evidenced by the NPD data. The known Néel temperature for the alabandite found in NPD occurs at approximately 75 K,[49] which rules out this 11

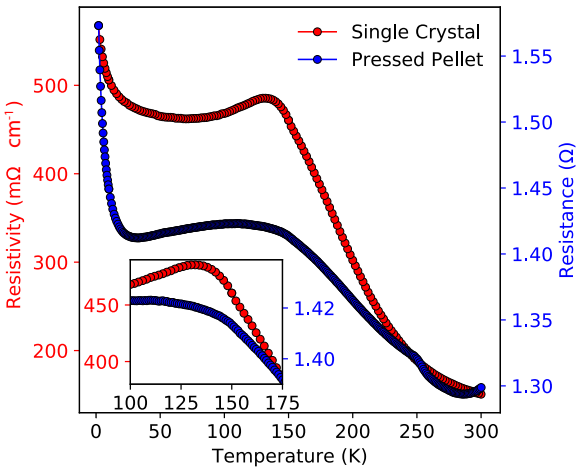

FIG. 7. Temperature dependent resistance of $KCuMnS_2$ pressed pellet (blue, bottom), and resistivity for a single crystal of $KCuMnS_2$ along the *ab*-plane (red, top). Semiconductor to metallic behavior is observed below 150 K, which is proximate to the onset of long-range magnetic ordering (approximately 160 K), before resuming semiconductor behavior.

K feature as arising from impurity.

C. Electrical resistivity and electronic structure

Measurements for the resistance of a pressed pellet and resistivity along the *ab*-plane of a single crystal of $KCuMnS_2$ are presented in Figure 7. Both samples show primarily semiconducting behavior with a distinct transition near 150 K. Below this transition, both samples exhibit metallic-like behavior since resistance (resistivity) both decrease with temperature until semiconductor behavior resumes at lower temperatures. For the polycrystalline sample, this occurs near 30 K, and for the single crystal near 80 K. The anomaly in the transport results is more more distinct in the single crystal sample (Figure 7 inset), which likely arises from powder averaging, although the transition at lower temperature is more distinct in the pressed pellet sample.

The anomaly in the resistivity of the $KCuMnS_2$ single crystal occurs near the Néel temperature of 160 K, indicating that long-range magnetic order leads to an increase in the conductivity of the sample. This is further supported by the lower temperature transition prominent in the powder sample which resumes semiconductor behavior around 30 K at the same time as the magnetic intensity from Figure 4 begins to saturate. We were not able to measure the resistivity along the *c*-axis for the single crystal sample of $KCuMnS_2$ due to the sample morphology and were unable to obtain consistent results for $KLiMnS_2$ samples.

Density functional theory (DFT) calculations were also performed for both $KCuMnS_2$ and $KLiMnS_2$ to help gain a better understanding of the electrical transport properties. The dispersion curve of the electronic states near the Fermi level at along major symmetry directions and density of state (DOS) from DFT for the simple layered checkerboard Néel type magnetic structure in Figure S2 can be seen in Figure 8 for both compounds. Unsurprisingly, given that the all the cations have either full or half-full shells, the electronic DOS shows both to be semiconductors with bandgaps near 0.5 eV for $KCuMnS_2$ and 0.8 eV for $KLiMnS_2$. Since the Fermi-level is on the edge of the valence band for both compounds, these materials would be more susceptible to hole doping to tune the electronic properties.

IV. DISCUSSION

A. Structure and bonding

With both sulfides crystallizing in the $I4/mmm$ space group, the only refineable structural parameter is the *z*-position for the 4*e* site of the sulfide anion. The effective ionic radii of Li^+ (0.59 Å) and Cu^+ (0.60 Å)[54] are very similar, yet the nature of the monovalent cation greatly effects the *z*-position of the sulfide anions and cell parameters. The S–*M*–S tetrahedral bond angles better illustrate this drastic change. While the CuS_4 tetrahedron has nearly ideal values of 109.22(4)° and 109.60(2)° for the S–*M*–S bond angles (from single crystal XRD at 250 K), the LiS_4 tetrahedron has bond angles of 112.6(2)° and 107.94(8)° (from NPD data at 200 K). Therefore, the ionic radii do not play a role in determining the key structural parameter in this system, but rather the electronics may be playing the larger role. A full $3d^{10}$ shell as opposed to a full $1s^2$ shell could more effectively hybridize with the sulfur $3p$ levels due to better matching of the orbital energy levels.

Because of the symmetry constraints of the crystal system, there is only one unique *M*–S bond distance in this system. Interestingly, while the S–*M*–S bond angles were drastically changed by the nature of *M*, the bond distance is unaffected. In $KMMnS_2$, the *M*–S interatomic distance is given by 2.4270(7) Å and 2.431(2) Å for *M* = Cu and Li, respectively. These distances are close to that of 2.439(3) Å reported by Bronger et al.[29] Nevertheless, the change in S–*M*–S bond angle causes an increase of the *a*-parameter and decrease of the *c*-parameter for *M* = Li with respect to *M* = Cu. This is due to the fact that the tetrahedral angle within the *ab*-plane increases, while that out of the plane decreases.

We conclude that the relevant structural changes from diffraction patterns demonstrate that ionic radii are not the only determining factor in these quaternary sulfides. The nature of *M* is quite important due to the orbitals that are engaged in bonding. The nearly ideal tetrahedron created by the Cu^+ will constrain the magnetic Mn^{2+} while this is not the case for Li^+. Covalent bonding is strengthened between metal and sulfur for the case

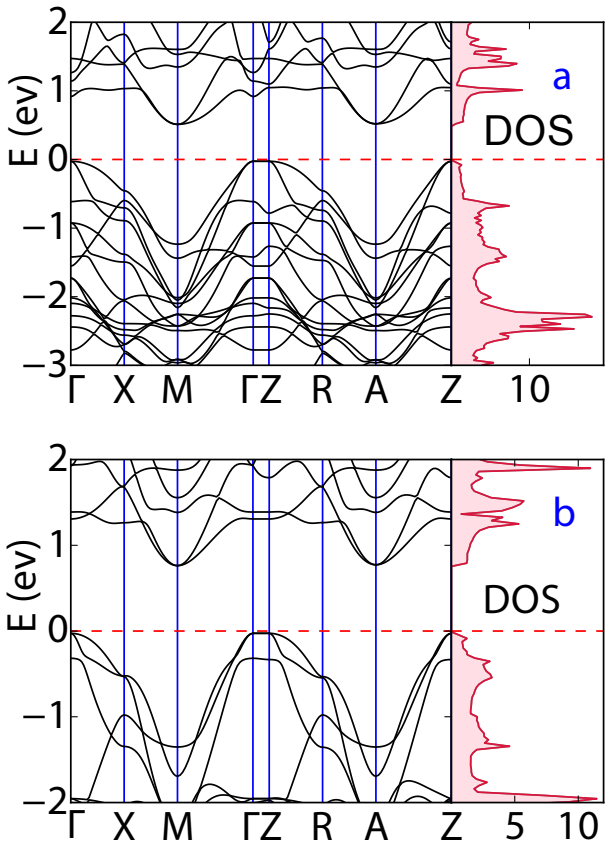

FIG. 8. Dispersion curves and DOS of the electronic states near the Fermi-level for $KCuMnS_2$ (a) and $KLiMnS_2$ (b) showing the Fermi-level on the edge of the valence band.

of $M = Cu^+$. Undoubtedly, this will have an effect on the crystal field splitting energies for the d^5 cations and the electronic structure, which we discuss next.

B. Electrical transport and sample preparation

Although transport measurements indicate that both sulfides are semiconducting, only the $M = Cu$ sample displayed a sufficiently small band gap to measure resistivity down to base temperature. It is apparent in the temperature dependence of the single crystal sample of $KCuMnS_2$ that the anomaly in the resistivity is related to the antiferromagnetic transition. A similar anomaly has been found in the parent superconductor $Fe_{1+x}Te$ for $x = 12\%$, whereby the T_N causes an anomaly in the semiconductor-type resistivity measurement.[55–60] This has been attributed to scattering from spin fluctuations that persist below the ordering temperature, and a similar phenomenon may be occurring with $KCuMnS_2$.

The predicted band gaps in $KCuMnS_2$ and $KLiMnS_2$ are 0.5 eV and 0.8 eV, respectively. Likely, the nearly ideal tetrahedral environment in $KCuMnS_2$ causes more orbital overlap between the Cu/Mn metal and S anions, thereby increasing the band width of the conduction band. Another notable difference in the calculated band structure is that the Cu d-states create more electronic states between 0 and -2 eV as evidenced by the dispersion curves in Figure 8. Therefore, a distribution of electronic DOS near the Fermi level is created by these extra states in the Cu compound.

The similarity of our $KCuMnS_2$ structure with that reported by Oledzka is in contrast with the noticeable differences between the resistivity measurements reported here and those of Oledzka et al.[24] The previous results by Oledzka are consistent with that of a highly doped, or degenerate semiconductor, with metallic behavior above 80 K, but with resistances too high to be called metallic. While the magnitude of the resistivity for each report is relatively consistent, even with the differences between how the samples were prepared for measurement (sintered vs pressed pellet and single crystal), our results are more in line with the $ACuCoS_2$ semiconductors also prepared by Oledzka et al.[27] Apart from the reduction in resistivity during the onset of the magnetic moment, not seen in $ACuCoS_2$, our resistivity measurements show semiconducting behavior.

The difference in the resistivity measurements between the two reports for $KCuMnS_2$ can be explained by the seemingly trivial differences between our synthesis and that of previous work.[24] washed the as-recovered powders with water, whereas we washed the excess flux with methanol. Washing with water could have removed some of the K^+ ions in the structure, as can readily happen with other known 122-type chalcogendies such as KCo_2Se_2.[61] Removal of K^+ from the lattice would oxidize the metal and therefore effectively hole doping the system. With sufficient lowering of the Fermi-level into the valence band, the compound may express metallic behavior. This semiconducting behavior is also present in the $ACuFeS_2$ compounds by Oledzka, though the values for resistivity were too great to measure below 200 K. The deviation from the predicted metallic behavior from electronic band calculations are partially explained by a non-ideal tetrahedral environment for the Cu/Fe site.

C. Comparison of AFM models

Although we could not determine the definitive antiferromagnetic structure of $KCuMnS_2$ from neutron diffraction, other evidence may point in favor one structure over the other. First, the stripe order would break 4-fold symmetry in the compound, as often happens with the 122-type iron arsenides.[62] In those parent-phases of the superconductors, the T_N is either coincident or near a tetragonal-to-orthorhombic phase transition.[63–67] Likewise, the $Fe_{1+x}Te$ system displays a structural phase transition near the Néel temperature. The above-mentioned compounds all display either single-stripe or double-stripe antiferromagnetic order.[56,57] However, this phase transition is clearly not the case in the quater-

nary 122-sulfides studied here. The lack of a structural transition upon AFM order strengthens the case for the non-collinear structure. The critical exponent of $\beta = 0.331(5)$ for the magnetization from the neutron measurements is closest the value found for an Ising spin system in a three-dimensional lattice (3D). A similar non-collinear structure was determined for the Mott-insulator $La_2O_2Fe_2OSe_2$, which was found to be a 2D Ising system.[68]

Clearly some AFM order is needed to explain the semiconducting behavior, and the DFT results offer guidance on the true state in the $KCuMnS_2$ system. The band structure and DOS in Figure S3 predict $KCuMnS_2$ to be metallic if AFM order is excluded. The AFM model (layered checkerboard) led to the electronic DOS of Figure 8, which shows $KCuMnS_2$ to be semiconducting. While simple to construct, this model is obviously wrong according to the neutron diffraction results. Therefore, we performed additional band structure calculations in order to understand how other magnetic structures may influence the electric properties. We constructed two additional AFM models. One model has the Cu and Mn cations ordered in a double striped fashion in order to construct the striped AFM order on the Mn site. The other model has Mn arranged so that it forms a tetramer that would support the non-collinear AFM models of Figure 6. Both models have a 2×2 magnetic unit cell and are illustrated in Figure S2.

In the case of $KCuMnS_2$, the two types of AFM order (striped and non-collinear) do not lead to qualitatively different electric properties from each other. However, their electronic DOS are quite different. As shown in the DOS of Figure S3, for the striped model, it appears that $KCuMnS_2$ is not quite a semiconductor but instead a metal with a very small Fermi surface. The Fermi level just crosses the top of the valence band. In the non-collinear AFM model, the same is true but there are some extra states near the valence band that would suggest a smaller band gap if it was a semiconductor. The total energies from the band structure calculations are presented in Table S1 which shows the striped order to be the lowest energy of all the AFM models. We must be careful in over interpreting these results, however, in that the Cu and Mn cations always remain disordered in $KCuMnS_2$ and the DFT results only reflect the case for particular types of cation ordering. From these limited calculations, however, the striped order would seem to be favored.

Determination of the correct magnetic structure could be aided by future experiments on the system. The most straightforward approach would be single crystal transport measurements such as angle-dependent magnetoresistance and/or angle dependent magnetization measurements. Furthermore, a comprehensive way to understand the structure would be polarized single crystal or powder neutron diffraction which would definitively allow for the magnetic structure to be solved.

D. Comparison with other 122-systems

Once again, it is interesting to compare the results here to those found previously on $KCuMnS_2$. Oledzka et al. observed a broad plateau just below room temperature for $KCuMnS_2$, which is attributed to short-range antiferromagnetic behavior.[24] They proposed that the suppression of magnetic ordering was due to the disruption caused by the Cu^+ ions in the square lattice even though there may be strong antiferromagnetic exchange between the Mn^{2+} ions. However, we did not find such a divergence between the ZFC and FC curves in our magnetic susceptibility measurements. Again, this may be due to how we processed the sample after synthesis and the spin glassy behavior may arrive from vacancies rather than the random distribution of Cu^+ cations. The random distribution of the M cations in the structure leading to clusters of Mn^{2+} is also noted as the cause for the reported divergence between ZFC and FC below 38 K, and attributed this to a spin-glassy transition.[24] However, such divergence was absent from our current measurements with the $KCuMnS_2$ system, suggesting lack of the spin-glass phase.

We also consider the closely related $KCuFeS_2$ and $KCuCoS_2$, which are isostructural. Oledzka found $KCuFeS_2$ to also be an antiferromagnet with a T_N of 40 K, although no neutron diffraction was ever carried out to investigate the possible order.[24] While a split in their ZFC and FC curves at low temperatures may suggest some spin glassiness from the random distributions of Fe and Cu cations, this explanation would not be consistent with the case of $KCuCoS_2$. In this compound the Co and Cu cations are also randomly distributed, yet the system undergoes a ferromagnetic transition near 120 K.[27]

Spin-glass behavior is not common for most of these 122-type quaternaries. $KCuCoS_2$, despite having the same random orientation of magnetic ions the d^8 Co instead undergoes a ferromagnetic transition around 120 K. In the case of $KCuCoS_2$, it is believed that c-axis interactions dominate above the T_c while ab-plane interactions make the overall order ferromagnetic below the T_c. This T_c can change due to the temperature of synthetic conditions similar to ours, dropping drastically to 50 K when the reaction temperature is increased from 720 °C to 900 °C possibly attributed to changes in the Co/Cu distribution, or sulfur vacancies.

Spin-glass behavior is also not observed in the AMn_2Pn_2 compounds that exhibit antiferromagnetic behavior, possibly higher than room temperature.[45,69–71] Their G-type order indicates Mn^{2+} in the high-spin tetrahedral coordination. This is in contrast to our NPD providing a 0.92(2) μ_B/Mn^{2+}, which indicates low-spin Mn^{2+} in a tetrahedral environment. Indeed this leads our results to more similarly resemble the class of isostructural AMn_2Pn_2 compounds. $BaMn_2Sb_2$ and $BaMn_2As_2$ have both shown themselves to be G-type collinear antiferromagnets, with no c-component to the magnetic moment.[45,69] The magnetic susceptibility can also be

highly anisotropic with respect to the *ab*-plane for these AMn$_2$Pn$_2$ compounds, featuring a clear feature in the susceptibility at the Néel temperature when measured parallel to the *c*-axis, that is much less pronounced when measured in the *ab*-plane.[45,48] A strong dominating *ab*-plane contribution to the magnetic susceptibility could contribute to the presence of only a subtle feature in our powder samples.

The notable difference here is that while $BaMn_2Sb_2$ has a T_N of 118 K, the T_N of $BaMn_2As_2$ is well above room temperature at 625 K.[70] While the magnitude of the magnetic moments for the AMn$_2$Pn$_2$ compounds is less than the nominal 5.0 μ_B/Mn for high spin Mn^{2+}, the values of roughly 3.75μ_B/Mn are still well above that for $KCuMnS_2$.[46,72–75] While this decrease for the pnictides is attributed to the strong spin dependent hybridization of the Mn 3*d* and As 4*p* orbitals, the reduction for $KCuMnS_2$ is likely similar to that of the Fe-122 compounds due to the itinerant nature of the magnetism. It is this itinerant nature that could help $KCuMnS_2$ resemble the high T_N pnictides. Our magnetic susceptibility data hinted at a high (above our room temperature capabilities) T_N antiferromagnet, though the lack of unindexed NPD peaks refutes the presence of any long-range ordering above 160 K.

V. CONCLUSION

$KCuMnS_2$ and $KLiMnS_2$ were prepared trough high temperature reaction from the respective K and Li carbonates with pure metals under a CS_2 in Ar flow. Single crystals of $KCuMnS_2$ were prepared via a melt of the unwashed powder in an evacuated ampule. From neutron diffraction data, we have proposed a striped pattern magnetic structure, as well as a non-colinear magnetic structure for $KCuMnS_2$, with alternating layers oriented antiferromagnetically with a T_N of 160.5 K. Both structures have their magnetic moment oriented along only the *ab*-plane and a moment that was refined to 0.92(2) μ_B/ Mn^{2+}. We have also shown that by substituting Li^+ for Cu^+, long range ordering of the magnetic moment is destroyed. A feature of the $KLiMnS_2$ NPD pattern could indicate some short range ordering, though it is not definitive as it could also be the result of inelastic scattering.

The magnetic susceptibility of $KCuMnS_2$ decreases with temperature, showing only a small feature near 160 K, until developing a curie tail near 40 K. Single crystal and pressed pellet powder samples of $KCuMnS_2$ show primarily semiconducting behavior for resistivity/resistance measurements respectively, except around the T_N of 160.5 K. Immediatly below 160 K, $KCuMnS_2$ shows metallic behavior until resuming semiconducting behavior when the moment saturates, indicating that long-range magnetic order aids in the conductivity of the sample. Band structure calculations show the Fermi-level at the edge of the valence band for both compounds would make them susceptible to hole-doping.

VI. ACKNOWLEDGMENTS

Research at the University of Maryland was supported by the NSF Career DMR-1455118 and the Department of Commerce under the NIST award 70NANB12H238. The identification of any commercial product or trade name does not imply endorsement or recommendation by the National Institute of Standards and Technology. The authors acknowledge the University of Maryland supercomputing resources (http://www.it.umd.edu/hpcc) made available for conducting the research reported in this paper. The part of the research that was conducted at ORNLs High Flux Isotope Reactor was sponsored by the Scientific User Facilities Division, Office of Basic Energy Sciences, US Department of Energy.

* efrain@umd.edu

[1] R. Hoffmann and C. Zheng, The Journal of Physical Chemistry **89**, 4175 (1985).
[2] R. Hoffmann, Angewandte Chemie International Edition in English **26**, 846 (1987).
[3] S. A. J. Kimber, A. Kreyssig, Y.-Z. Zhang, H. O. Jeschke, R. Valenti, F. Yokaichiya, E. Colombier, J. Yan, T. C. Hansen, T. Chatterji, R. J. McQueeney, P. C. Canfield, A. I. Goldman, and D. N. Argyriou, Nature Materials **8**, 471 (2009), arXiv:0912.2376.
[4] S. Peschke, T. Stürzer, and D. Johrendt, Zeitschrift für anorganische und allgemeine Chemie **640**, 830 (2014).
[5] M. V. Sadovskii, E. Z. Kuchinskii, and I. A. Nekrasov, in *Journal of Magnetism and Magnetic Materials*, Vol. 324 (Elsevier, 2012) pp. 3481–3486, arXiv:1106.3707.
[6] R. Mittal, S. K. Mishra, S. L. Chaplot, S. V. Ovsyannikov, E. Greenberg, D. M. Trots, L. Dubrovinsky, Y. Su, T. Brueckel, S. Matsuishi, H. Hosono, and G. Garbarino, Physical Review B - Condensed Matter and Materials Physics **83**, 054503 (2011), arXiv:1007.2320.
[7] D. P. Shoemaker, D. Y. Chung, H. Claus, M. C. Francisco, S. Avci, A. Llobet, and M. G. Kanatzidis, Physical Review B **86**, 184511 (2012).
[8] D. Yuan, N. Liu, K. Li, S. Jin, J. Guo, and X. Chen, Inorganic Chemistry **2**, 13187 (2017).
[9] I. A. Nekrasov and M. V. Sadovskii, JETP Letters **99**, 598 (2014), arXiv:1405.5677.
[10] D. C. Johnston, Advances in Physics **59**, 803 (2010).
[11] J. Paglione and R. L. Greene, Nature Physics **6**, 645 (2010).
[12] Y. Mizuguchi and Y. Takano, Journal of the Physical Society of Japan **79**, 102001 (2010).
[13] X. H. Niu, S. D. Chen, J. Jiang, Z. R. Ye, T. L. Yu, D. F. Xu, M. Xu, Y. Feng, Y. J. Yan, B. P. Xie, J. Zhao, D. C. Gu, L. L. Sun, Q. Mao, H. Wang, M. Fang, C. J. Zhang, J. P. Hu, Z. Sun, and D. L. Feng, Physical Review B **93**, 054516 (2016).

[14] Q. Si, R. Yu, and E. Abrahams, Nature Reviews Materials **1**, 16017 (2016).

[15] A. Newmark, G. Huan, M. Greenblatt, and M. Croft, Solid State Communications **71**, 1025 (1989).

[16] G. Huan, M. Greenblatt, and K. Ramanujachary, Solid State Communications **71**, 221 (1989).

[17] J. Yang, B. Chen, H. Wang, Q. Mao, M. Imai, K. Yoshimura, and M. Fang, Physical Review B **88**, 064406 (2013).

[18] R. Lizárraga, S. Ronneteg, R. Berger, A. Bergman, P. Mohn, O. Eriksson, and L. Nordström, Physical Review B **70**, 024407 (2004).

[19] J. Yang, B. Chen, H. Wang, Q. Mao, M. Imai, K. Yoshimura, and M. Fang, Physical Review B - Condensed Matter and Materials Physics **88**, 064406 (2013), arXiv:1305.0123.

[20] J. An, A. S. Sefat, D. J. Singh, and M.-H. Du, Phys. Rev. B **79**, 075120 (2009).

[21] Y. Singh, M. A. Green, Q. Huang, A. Kreyssig, R. J. McQueeney, D. C. Johnston, and A. I. Goldman, Phys. Rev. B **80**, 100403 (2009).

[22] D. C. Johnston, R. J. McQueeney, B. Lake, A. Honecker, M. E. Zhitomirsky, R. Nath, Y. Furukawa, V. P. Antropov, and Y. Singh, Phys. Rev. B **84**, 094445 (2011).

[23] X. Lai, S. Jin, X. Chen, T. Zhou, T. Ying, H. Zhang, and S. Shen, Materials Express **4**, 343 (2014).

[24] M. Oledzka, C. Lee, K. Ramanujachary, and M. Greenblatt, Materials Research Bulletin **32**, 889 (1997).

[25] M. Oledzka, K. Ramanujachary, and M. Greenblatt, Mater. Res. Bull. **33**, 855 (1998).

[26] M. Oledzka, K. V. Ramanujachary, and M. Greenblatt, Materials Research Bulletin **31**, 1491 (1996).

[27] M. Oledzka, J.-G. Lee, K. Ramanujachary, and M. Greenblatt, Journal of Solid State Chemistry **127**, 151 (1996).

[28] M. Oledzka, K. V. Ramanujachary, and M. Greenblatt, Chemistry of Materials **10**, 322 (1998).

[29] D. Schmitz and W. Bronger, Zeitschrift fr anorganische und allgemeine Chemie **553**, 248 (1987).

[30] W. Bronger, H. Hardtdegen, M. Kanert, P. Müller, and D. Schmitz, Zeitschrift für anorganische und allgemeine Chemie **622**, 313 (1996).

[31] J. Lynn, Y. Chen, S. Chang, Y. Zhao, S. Chi, W. Ratcliff II, B. Ueland, and R. Erwin, Journal of Research of the National Institute of Standards and Technology **117**, 60 (2012).

[32] B. J. Campbell, H. T. Stokes, D. E. Tanner, and D. M. Hatch, Journal of Applied Crystallography **39**, 607 (2006).

[33] R. W. Cheary and A. Coelho, Journal of Applied Crystallography **25**, 109 (1992).

[34] G. M. Sheldrick, Acta Crystallographica Section C Structural Chemistry **71**, 3 (2015).

[35] P. Hohenberg and W. Kohn, Physical Review **136**, B864 (1964).

[36] W. Kohn and L. J. Sham, Physical Review **137**, A1697 (1965).

[37] G. Kresse and J. Furthmüller, Physical Review B **54**, 11169 (1996).

[38] G. Kresse and J. Furthmüller, Computational Materials Science **6**, 15 (1996).

[39] G. Kresse and J. Hafner, Physical Review B **47**, 558 (1993).

[40] G. Kresse and J. Hafner, Physical Review B **48**, 13115 (1993).

[41] P. E. Blöchl, Physical Review B **50**, 17953 (1994).

[42] J. P. Perdew, K. Burke, and M. Ernzerhof, Physical Review Letters **77**, 3865 (1996).

[43] H. J. Monkhorst and J. D. Pack, Physical Review B **13**, 5188 (1976).

[44] See Supplemental Material at [URL will be inserted by publisher] for the temperature dependence of lattice parameters for $KCuMnS_2$, and additional DFT calculations.

[45] P. Das, N. S. Sangeetha, A. Pandey, Z. A. Benson, T. W. Heitmann, D. C. Johnston, A. I. Goldman, and A. Kreyssig, Journal of Physics: Condensed Matter **29**, 035802 (2017), arXiv:1605.02004.

[46] S. L. Brock, J. Greedan, and S. M. Kauzlarich, Journal of Solid State Chemistry **113**, 303 (1994).

[47] S. L. Brock, J. Greedan, and S. M. Kauzlarich, Journal of Solid State Chemistry **109**, 416 (1994).

[48] N. S. Sangeetha, A. Pandey, Z. A. Benson, and D. C. Johnston, Physical Review B **94**, 094417 (2016).

[49] L. Corliss, N. Elliott, and J. Hastings, Physical Review **104**, 924 (1956).

[50] R. Tappero, P. Wolfers, and A. Lichanot, Chemical Physics Letters **335**, 449 (2001).

[51] C. G. Shull, W. A. Strauser, and E. O. Wollan, Physical Review **83**, 333 (1951).

[52] W. L. Roth, Physical Review **110**, 1333 (1958).

[53] J. M. Hastings, N. Elliott, and L. M. Corliss, Physical Review **115**, 13 (1959).

[54] R. D. Shannon and C. T. Prewitt, Acta Crystallographica Section B Structural Crystallography and Crystal Chemistry **25**, 925 (1969).

[55] E. E. Rodriguez, P. Zavalij, P. Hsieh, and M. A. Green, Journal of the American Chemical Society **132**, 10006 (2010).

[56] P. Zajdel, P. Hsieh, E. E. Rodriguez, N. P. Butch, J. D. Magill, J. Paglione, P. Zavalij, M. R. Suchomel, and M. A. Green, Journal of the American Chemical Society **132**, 13000 (2010).

[57] E. E. Rodriguez, C. Stock, P. Zajdel, K. L. Krycka, C. F. Majkrzak, P. Zavalij, and M. A. Green, Physical Review B **84**, 064403 (2011).

[58] C. Stock, E. E. Rodriguez, M. A. Green, P. Zavalij, and J. A. Rodriguez-Rivera, Physical Review B **84**, 045124 (2011).

[59] E. E. Rodriguez, D. A. Sokolov, C. Stock, M. A. Green, O. Sobolev, J. A. Rodriguez-Rivera, H. Cao, and A. Daoud-Aladine, Physical Review B **88**, 165110 (2013).

[60] C. Stock, E. E. Rodriguez, O. Sobolev, J. A. Rodriguez-Rivera, R. A. Ewings, J. W. Taylor, A. D. Christianson, and M. A. Green, Physical Review B **90**, 121113 (2014).

[61] X. Zhou, B. Wilfong, H. Vivanco, J. Paglione, C. M. Brown, and E. E. Rodriguez, Journal of the American Chemical Society **138**, 16432 (2016).

[62] E. E. Rodriguez, C. Stock, K. L. Krycka, C. F. Majkrzak, P. Zajdel, K. Kirshenbaum, N. P. Butch, S. R. Saha, J. Paglione, and M. A. Green, Physical Review B **83**, 134438 (2011).

[63] J. Zhao, Q. Huang, C. de la Cruz, S. Li, J. W. Lynn, Y. Chen, M. A. Green, G. F. Chen, G. Li, Z. Li, J. L. Luo, N. L. Wang, and P. Dai, Nature Materials **7**, 953 (2008).

[64] C. Liu, T. Kondo, N. Ni, A. D. Palczewski, A. Bostwick, G. D. Samolyuk, R. Khasanov, M. Shi, E. Rotenberg, S. L. Bud'ko, P. C. Canfield, and A. Kaminski, Physical Review Letters **102**, 167004 (2009).

[65] M. Rotter, M. Pangerl, M. Tegel, and D. Johrendt, Angewandte Chemie International Edition **47**, 7949 (2008).

[66] D. Johrendt and R. Pöttgen, Physica C: Superconductivity **469**, 332 (2009).
[67] J. Wu, J. Lin, X. Wang, Q. Liu, J. Zhu, Y. Xiao, P. Chow, and C. Jin, (2014), 10.1073/pnas.1310286110, arXiv:1402.4086.
[68] E. E. McCabe, C. Stock, E. E. Rodriguez, A. S. Wills, J. W. Taylor, and J. S. O. Evans, Physical Review B **89**, 100402 (2014).
[69] Y. Singh, A. Ellern, and D. C. Johnston, Physical Review B **79**, 094519 (2009), arXiv:arXiv:0901.3370v2.
[70] M. Ramazanoglu, A. Sapkota, A. Pandey, J. Lamsal, D. Abernathy, J. Niedziela, M. Stone, R. Salci, D. Acar, F. Oztirpan, S. Ozonder, A. Kreyssig, A. Goldman, D. Johnston, and R. McQueeney, Physica B: Condensed Matter , 1 (2017).
[71] A. Pandey, R. S. Dhaka, J. Lamsal, Y. Lee, V. K. Anand, A. Kreyssig, T. W. Heitmann, R. J. McQueeney, A. I. Goldman, B. N. Harmon, A. Kaminski, and D. C. Johnston, Physical Review Letters **108**, 087005 (2012), arXiv:arXiv:1110.5546v2.
[72] D. E. McNally, J. W. Simonson, J. J. Kistner-Morris, G. J. Smith, J. E. Hassinger, L. DeBeer-Schmitt, A. I. Kolesnikov, I. A. Zaliznyak, and M. C. Aronson, Physical Review B **91**, 180407 (2015), arXiv:arXiv:1505.06153v1.
[73] Q. D. Gibson, H. Wu, T. Liang, M. N. Ali, N. P. Ong, Q. Huang, and R. J. Cava, Physical Review B **91**, 085128 (2015).
[74] W. Ratcliff II, A. Lima Sharma, A. Gomes, J. Gonzalez, Q. Huang, and J. Singleton, Journal of Magnetism and Magnetic Materials **321**, 2612 (2009).
[75] C. Bridges, V. Krishnamurthy, S. Poulton, M. Paranthaman, B. Sales, C. Myers, and S. Bobev, Journal of Magnetism and Magnetic Materials **321**, 3653 (2009)
.